Murine models for triple-negative breast cancer with differential responsiveness to immunotherapy

Thomas J Kalantzakos,[1] Yufan Zhou,[1] Xingyu Liu,[1] Joshua Proehl,[1] Cameron Durfee,[1] Ian Tamayo[1], Nuri Alpay Temiz,[2,3] Benjamin Troness,[1] Anusha Soni,[1] Harshita B Gupta,[1,#] Reuben S Harris[1,4,#]

[1] Department of Biochemistry and Structural Biology, Long School of Medicine, University of Texas Health San Antonio, San Antonio, Texas, USA 78229

[2] Institute for Health Informatics, University of Minnesota, Minneapolis, Minnesota, USA, 55455

[3] Masonic Cancer Center, University of Minnesota, Minneapolis, Minnesota, USA, 55455

[4] Howard Hughes Medical Institute, University of Texas Health San Antonio, San Antonio, Texas, USA 78229

[#]Correspondence: GuptaH@uthscsa.edu or rsh@uthscsa.edu

Manuscript contents: 251 word abstract, 5478 word main text (excluding abstract, references and legends), 5 main figures, 2 supplementary tables, and 4 supplementary figures

ABSTRACT

Background Breast cancer is the most common cancer diagnosis in women. Clinical studies with triple-negative breast cancer (TNBC) are encouraging for immunotherapy combined with chemotherapy (αPD-1 with paclitaxel and/or carboplatin). However, additional clinical advances may be accelerated by leveraging preclinical TNBC models including syngeneic mammary tumor cell lines. Here, we report two syngeneic mammary tumor cell lines that exhibit differential

responsiveness to immunotherapy *in vivo*.

Methods Spontaneous mammary tumors from C57BL/6J *MMTV-Cre Trp53*$^{fl/+}$ animals were passaged serially in cell culture and *in vivo* in the mammary fat pad of fully wildtype animals. The resulting lines, MM001i and MM008i, lost *Trp53* and formed 1000 mm^3 tumors in the mammary fat pad within 21-28 days. Tumors from each group were analyzed for their response to αPd-1 and αCtla-4 immunotherapy, infiltrating immune populations, and transcriptional profiles.

Results Despite originating from the same genetic background, these lines exhibit differential responses to immunotherapy. For αPd-1 therapy, MM001i is poorly responsive and MM008i is strongly responsive with near-complete tumor regression. In comparison, both MM001i and MM008i respond rapidly to αCtla-4 therapy. Both models express unique tumor antigens as evidenced by immunity to subsequent engraftments. Primary MM008i tumors exhibit greater T cell infiltration, and CD8-positive T lymphocytes are required for αPd-1 responses. Cancer epithelial cells within MM008i tumors demonstrate a greater abundance of Pd-l1 expressing cells, correlating with observations in human TNBC where PD-L1 expression is a biomarker for αPD-1 response.

Conclusions These TNBC models are promising for further mechanistic studies and testing future single and combinatorial therapies.

WHAT IS ALREADY KNOWN ON THIS TOPIC

Immunotherapies such as αPD-1 have demonstrated modest clinical benefit for triple negative breast cancer (TNBC) patients with high PD-L1 expression. To improve therapy efficacy, there is a critical need to better understand mechanisms of sensitivity and resistance. Syngeneic models are a valuable tool for preclinical mechanistic studies of new therapeutics and immunotherapy *in vivo*. However, these models are rare, and those that exist are poorly responsive to immunotherapy and offer limited potential for mechanistic studies.

51 **WHAT THIS STUDY ADDS**

52 We generate two new syngeneic TNBC cell models derived from *Trp53*$^{fl/+}$ background in C57BL/6
53 mice. Despite a shared initial genotype and responsiveness to αCtla-4 therapy, these tumor lines
54 are differentially responsive to αPd-1 therapy and demonstrate major differences in infiltrating
55 immune populations.

56

57 **HOW THIS STUDY MIGHT AFFECT RESEARCH, PRACTICE, OR POLICY**

58 These new syngeneic model systems can be leveraged to better understand immunotherapy
59 responses and immune microenvironments in a fully immune competent setting, enabling future
60 mechanistic and therapeutic studies.

61

62 **INTRODUCTION**

63 Breast cancer is the most commonly diagnosed malignancy worldwide and a leading
64 cause of cancer-related death in women.[1, 2] Clinically, breast cancer is characterized based on
65 expression of estrogen receptor (ER), progesterone receptor (PR), and/or human epidermal
66 growth factor receptor 2 (HER2). Triple negative breast cancer (TNBC) lacks expression of these
67 three markers, accounts for 15-20% of breast cancer diagnoses, and is associated with poor
68 clinical outcomes.[3] For example, 30-40% of TNBC patients exhibit tumor recurrence within 3-5
69 years of the initial diagnosis and treatment.[4, 5] The most common genetic defect in TNBC is
70 mutation of *TP53* (hereafter *p53*) in 75-80% of cases,[6, 7] with most tumors incurring full loss-of-
71 function alleles.[8] TNBC tumors are highly heterogeneous and often subdivided into six molecular
72 clusters: basal-like 1, basal-like 2, immunomodulatory, mesenchymal, mesenchymal stem-like,
73 and luminal androgen receptor subtypes.[9]

74 Several clinical trials have demonstrated the benefit of immunotherapy approaches in
75 TNBC, particularly through monoclonal antibody (mAb) targeting of programmed cell death

76 protein 1 (PD-1) and cytotoxic T-lymphocyte antigen 4 (CTLA-4). The efficacy of immunotherapy,
77 particularly αPD-1, in combination with chemotherapy, is becoming established in both primary
78 and metastatic TNBC settings. In the KEYNOTE-522 clinical trial, adding αPD-1 to neoadjuvant
79 chemotherapy (paclitaxel and carboplatin followed by doxorubicin/epirubicin and
80 cyclophosphamide) in early TNBC improved pathological complete response from 51% to 65%.[10]
81 Further, the KEYNOTE-355 trial, conducted on advanced TNBC patients, demonstrated a robust
82 increase in overall survival when combining αPD-1 and chemotherapy in patients with high
83 programmed cell death-ligand 1 (PD-L1) expression.[11] Emerging studies are also evaluating
84 combination immunotherapy approaches. For example, the BELLINI trial is investigating dual
85 inhibition of αPD-1 and αCTLA-4, showing signs of efficacy in early-stage TNBC.[12] Additionally,
86 bi-specific antibodies targeting αPD-1 and αCTLA-4 combined with paclitaxel have shown
87 survival benefits for TNBC patients in the metastatic setting.[13] Additional trials are ongoing that
88 combine immunotherapies with radiation therapy and/or chemotherapy (*e.g.*, NCT04683679,
89 NCT05491226, NCT06472583). However, despite these recent advances, a large subset of
90 TNBC patients still suffers from disease progression, which warrants further mechanistic and
91 therapeutic studies.

92 Syngeneic murine models are useful for preclinical evaluation of candidate therapeutics
93 *in vivo.* To date, only a few murine syngeneic models for TNBC have been reported. The first,
94 E0771, was derived in 1955 from a spontaneously occurring breast adenocarcinoma in a C57BL/6
95 background.[14] Treatment of this model with αPd-1 leads to partial tumor regression[15] and
96 enhanced efficacy when combined with other agents.[16] αPd-1 and αCtla-4 therapies also
97 associate with increases in circulating $Cd8^+$ T lymphocytes in this model.[16, 17] However, it is an
98 older model and reports conflict on several key properties including genotype and hormone
99 receptor status.[18-20] Another commonly used line is 4T1, isolated from a metastatic tumor in a
100 BALB/c animal.[21] However, this line is poorly responsive to immunotherapy due at least in part to

101 a Th2-biased immune response.[22, 23] Other models, such as PyMT,[24] AT-3,[25] and WT145[26] are
102 additionally complicated by viral transgenes and/or chemical exposures.

103 Here, we report the development of two new cell lines, MM001-immunoconditioned
104 (MM001i) and MM008i, derived from mammary tumors that arose on C57BL/6J background.
105 Briefly, the primary mammary tissues were engineered to be heterozygous for *Trp53*, but the
106 second copy was lost during tumor development in both cell lines. Serial passage in culture and
107 *in vivo* resulted in MM001i and MM008i, which form 1000 mm^3 tumors approximately 21-28 days
108 after engraftment. Both lines are negative for Er, Pr, and Her2 (triple-negative) and provoke anti-
109 tumor immune responses, as evidenced by immune memory formation and acquired resistance
110 to additional challenge by the same tumor cell line. Both lines also respond to αCtla-4
111 immunotherapy, but only MM008i responds to αPd-1 immunotherapy. This differential
112 responsiveness is dependent on $Cd8^+$ T lymphocytes and may be attributable to improved
113 immune cell infiltration in MM008i tumors ($Cd45^+$ immune cells, $Cd8^+$ T lymphocytes). Taken
114 together, these syngeneic tumor lines constitute new models for TNBC and provide a foundation
115 for additional studies on molecular mechanisms and responsiveness of different
116 immunotherapies.

117

118 **MATERIALS AND METHODS**

119 **Mouse Care**

120 All animal studies were approved by the University of Texas Health San Antonio (UT
121 Health) Institutional Animal Care and Use Committee (IACUC Protocol ID: 20220056AR) and
122 conducted in accordance with ARRIVE guidelines 2.0[27]. "Guide for the care and use of laboratory
123 animals" guidelines were followed, and the study adhered to the principles of 3Rs (Replace,
124 Reduce, and Refine). The Lab Animal Resources (LAR) facilities at UT Health are AAALAC
125 (accredited unit: #000341) and USDA (registration number: 74-R-0071) approved. 24/7/365 LAR

126 staff include veterinarians, facility staff, and animal technicians for services including complete
127 husbandry, routine monitoring, examination of mice health and supportive care. 3-5 animals per
128 cage were housed in specific pathogen-free conditions maintained at 22°C under a standard 12-
129 hour light/dark cycle and given food and water *ad libitum*. Initial breeder pairs for WT (Jax strain
130 000664) and NOD.Cg-Prkdc^{scid}Il2rg^{tm1Wj1}/SzJ (nonobese diabetic/severe combined
131 immunodeficiency (NOD/SCID)/IL2Rγ KO, NSG, Jax strain 005557) mice were purchased from
132 Jackson Laboratory (Bar Harbor, ME, USA), and then propagated in-house. NSG mice were
133 maintained under sterile conditions. 8-10 weeks-old mice were enrolled for tumor studies. All
134 immunocompetent mice were on C57BL/6J background, and only females were used for
135 mammary tumor experiments.

136 Mice were checked one day post-injection, and then twice a week for tumor growth,
137 morbidity, weight loss, and dehydration. Mice were euthanized if they were in distress, lost >20%
138 body weight, showed a body score <2, and/or reached experimental end points such as 1000
139 mm^3 tumor volumes. The signs of distress included but were not limited to dehydration, cachexia,
140 weakness, ruffled body fur, or hunched back. Euthanasia was done as recommended by the
141 American Veterinary Medical Association guidelines for the Euthanasia of Animals. Briefly, mice
142 were subjected to inhalation of 99% pure CO_2 with a fill rate of 30-70% chamber volume/minute
143 for 2 minutes followed by cervical dislocation. Anesthesia was not used for the experiments
144 performed for this study.

145

146 **Tumor harvesting from mice**

147 *MMTV-Cre p53*$^{fl/+}$ mice were bred initially at the University of Minnesota and subsequently
148 at UT Health prior to the present studies. Genotypes were confirmed via PCR[28] using primers:
149 1F: 5'-TAACACTCTTGGGATGCTGAG-3', 10F: 5'-AAGGGGTATGAGGGACAAGG-3', and 10R: 5'-
150 GAAGACAGAAAAGGGGAGGG-3'. Spontaneously arising primary mammary tumors in these

151 mice were extracted under sterile conditions, and single-cell suspensions were made by tumor
152 dissection and mechanical dissociation. Cells were transferred to a cell culture flask in RPMI-
153 1640 (Thermo Fisher Scientific, Waltham, MA, USA) supplemented with 10% fetal bovine serum
154 (FBS, Thermo Fisher Scientific) and 1% penicillin-streptomycin (complete medium, Thermo
155 Fisher Scientific). Once the cells reached 80% confluence, cells were harvested by 0.05% trypsin-
156 EDTA (Gibco, Thermo Fisher Scientific) for injecting in mice. Freeze downs were made
157 simultaneously in 90% FBS/10% DMSO (Sigma-Aldrich, St. Louis, MO, USA).
158

159 **Serial passage to develop conditioned cell lines**

160 Cells were trypsinized, washed with endotoxin-free, sterile phosphate-buffered saline
161 (PBS) and combined at 1:1 ratio with Cultrex Basement Membrane Extract, PathClear (R&D
162 Systems, Minneapolis, MN, USA) for a final cell count as indicated (2.5 or 5 x 10^6 cells) in a final
163 volume of 100 µL per injection. Cells were injected subcutaneously or into the 4th inguinal
164 mammary fat pads of mice. Initial engraftments were conducted in both WT and NSG mice. As
165 tumors successfully engrafted in both strains, subsequent engraftments for serial passage were
166 conducted in WT mice alone. At day 7, tumors were measured using Vernier caliper (Thermo
167 Fisher Scientific) and then monitored twice a week until reaching a volume of 1000 mm^3 using the
168 equation $V=0.5 \times L \times W^2$.[29] Tumors reaching 1000 mm^3 were subsequently isolated post-humane
169 mouse euthanasia. The process was repeated for at least two rounds per cell line.
170

171 **Flow cytometry**

172 MM001i or MM008i cells were plated overnight in 6-well plates in complete medium (3 x
173 10^5 cells/well). Cells were then incubated with fresh complete medium supplemented with either
174 vehicle or interferon-gamma (Ifn-γ) (R&D Systems) for 24 hours. Cells were harvested and
175 counted using the Countess cell counter (Thermo Fisher Scientific). 2 x 10^6 cells per condition
176 were analyzed for subsequent steps. Cells were washed with PBS, stained for live/dead dye

177 (Zombie Yellow Fixable Viability dye) in PBS for 40 min at 4°C in the dark. Cells were washed in
178 1x PBS and incubated with anti-Cd16/32 (BioLegend, San Diego, CA, USA) in flow buffer (PBS
179 + 2% FBS) to prevent non-specific antibody binding for 30 minutes at 4ºC, followed by incubation
180 with anti-mouse Pd-l1 (PE, clone 10F.9G2), H2-Kb (Pacific Blue), or matched isotype controls
181 (BioLegend). Cells were fixed in 0.4% buffered formalin. Cells were acquired using BD
182 LSRFortessa (BD Biosciences, San Juan, CA, USA) and analyzed using FACSDiva and FlowJo
183 10.10.0 (BD Biosciences).
184
185 **Immunotherapy experiments**
186 2.5 x 10^6 MM001i or MM008i cells were suspended in 50 µL endotoxin-free PBS. An equal
187 volume of basement membrane was added to reach a final volume of 100 µL/injection. For all
188 immunotherapy experiments, mice were randomized manually to equalize numbers across
189 treatment groups. Mice with no palpable tumor by day 7 were excluded from study due to likely
190 failed injection. Each mouse received two injections (one per inguinal mammary fat pad). On day
191 7, an initial tumor measurement was taken as previously described. Tumors were monitored twice
192 a week, and the mice were euthanized when tumors reached 1000 mm^3, or when they displayed
193 signs of distress. 7 days post-injection, each mouse received an intraperitoneal (i.p.) injection of
194 100 µg of αPd-1 (catalog no. BE0146, clone RMP1-14, BioXCell NH, USA), αCtla-4 (catalog no.
195 BE0131, clone 9H10, BioXCell), a combination of the two, or their respective isotype controls
196 (catalog # BE0089 and BE0087, BioXCell). Mice injected with MM001i received two additional
197 treatments on days 12 and 19.
198
199 **Memory response experiments**
200 WT mice with complete tumor regression in response to immunotherapy were enrolled in
201 memory rechallenge experiments. 90 days after the last tumor evaluation, mice were reinjected
202 with 2.5 million cells of the initial cell line at the same inguinal mammary fat pad. No further

203 treatments were administered. Tumors were measured beginning 7 days post-injection and
204 monitored as above until the endpoint was reached. The control group consisted of age-matched,
205 naïve, previously unchallenged WT mice injected with the same tumor cell line as the rechallenge
206 group but not treated with any immunotherapy agent.
207
208 **Immunohistochemistry**
209 IHC was performed as previously described.[30] In brief, FFPE tissues and cell pellets were
210 sectioned at 4 μm and mounted on positively charged glass slides. The slides were deparaffinized
211 at 65°C for 20 minutes, rehydrated with three 5-minute washes in CitriSolv (Decon Labs,
212 Swedeland, Pennsylvania, USA) followed by 3-minute washes in graded ethanol to 80%, and
213 finished with a 5-minute wash in running water. Antigen retrieval was performed in 1x Reveal
214 Decloaker (Biocare Medical, Pacheco, California, USA) by steaming for 35 minutes and returned
215 to room temperature with 20 minutes off the steamer. The slides were washed for 5 minutes in
216 running water and then in tris-buffered saline with 0.1% tween (TBST, Thermo Fisher Scientific).
217 Endogenous peroxidase activity was suppressed by soaking slides in 3% H_2O_2 diluted in TBST
218 for 10 minutes, followed by a 5-minute wash in running water. The slides were soaked in
219 Background Sniper (Biocare Medical) for 15 minutes, immediately followed by overnight
220 incubation of primary antibody diluted using 10% Sniper in TBST at 4°C. The following primary
221 antibodies were used: αEr (Catalog no. AB32063, 1:2000, Abcam, Cambridge, UK), αPr (Catalog
222 no. 25871-AP-1, 1:10000, ProteinTech, Rosemont, Illinois, USA), αHer2 (Catalog no. CST2165S,
223 1:1000, Cell Signaling Technologies, Danvers, Massachusetts, USA), αCd3 (Catalog no.
224 AB135372, 1:250, Abcam), and αCd19 (Catalog no. AB317335, 1:600, Abcam). After overnight
225 incubation, the slides are brought to room temperature and washed in TBST for 5 minutes. Next,
226 they were incubated with Novolink Polymer (Lieca Biosystems, Deer Park, Illinois, USA) for 30
227 minutes and developed using Novolink DAB substrate kit (Lieca Biosystems) for 5 minutes. Slides

228 were immediately washed in running water to quench substrate development and counterstained
229 10 minutes using Mayer's hematoxylin solution (Electron Microscopy Sciences, Hatfield,
230 Pennsylvania, USA). Slides were then dehydrated in degraded alcohols and CitriSolv and then
231 cover-slipped using Permount mounting media (Fisher Scientific).
232

233 **Immune cell infiltration analysis by IHC**

234 MM001i and MM008i sections were used to assess the infiltration of T and B lymphocytes
235 in n=4-5 tumors. T cells and B cells were visualized using αCd3 and αCd19 antibodies
236 respectively, as described above. T cell and B cell densities were calculated using QuPath v0.5.1
237 bioimage analysis software using the positive cell detection algorithm. 5 random uniform regions
238 of interest (ROIs) were selected within each tumor section and cell density was averaged for all
239 ROIs per tumor.
240

241 **Immune cell infiltration analysis by flow cytometry**

242 Mice were euthanized, and tumors were harvested once the mean group volume reached
243 750 mm^3. Tumors were digested, and single-cell suspensions were made using 0.3 mg Liberase
244 (Thermo Fisher Scientific) and 0.2 mg DNase I (Sigma-Aldrich) per tumor in incomplete RPMI-
245 1640. Tumors were mechanically dissociated, minced and incubated with shaking at 37°C for 30
246 minutes. Cell suspensions were harvested, passed through 70 μM strainers, and counted. 5×10^6
247 cells were stained for surface markers as above. Cells were incubated with αCd16/32 to prevent
248 non-specific antibody binding as above, followed by staining with αCd45 (FITC), αCd3 (PE-Cy7),
249 αCd8 (APC-Cy7), αCd4 (Bv786), αCd62l (Bv711), αPd-1 (PerCP-Cy5), αCd44 (Pacific Blue),
250 αTim3 (APC), or αGr1 (Bv786), αCd86 (APC-Cy7), αCd11c (PE), αCd11b (PerCP-Cy5), αB220
251 (AF700), αNK1.1 (APC) post live/dead staining (Zombie Yellow Fixable Viability dye). All
252 antibodies and Zombie Yellow Fixable Viability dye were purchased from BioLegend. Cells were

253 washed, fixed in 0.4% buffered formalin, and analyzed as mentioned above.

254

255 **$CD8^+$ neutralization experiments**

256 2.5 x 10^6 MM008i cells were injected into the mammary fat pads of immunocompetent WT
257 mice as previously described. On day 6, initial tumor measurements were taken, and mice were
258 randomized into groups. On days 6, 9, and 12, each mouse received an i.p. injection of 200 µg of
259 αCd8 antibody (catalog no. BE0004-1, clone 53-6.7, BioXCell) or its isotype control (catalog no.
260 BE0089, clone 2A3, BioXCell). On day 7, each mouse received a single i.p. injection of 100 µg of
261 αPd-1 or its isotype control, as previously described. Tumors were measured biweekly, and mice
262 were euthanized at day 25 or when tumor volumes reached 1000 mm^3. At day 13 and before
263 complete tumor regression, a small subset of tumors representing each treatment group were
264 isolated to assess immune infiltration of $CD8^+$ T lymphocytes by immunohistochemistry.

265

266 **Bulk RNA-sequencing of MM001i and MM008i cell lines and tumors**

267 RNA from two biological replicates each of MM001i and MM008i grown in culture were
268 isolated using the Qiagen RNeasy Mini Kit (Qiagen, Hilden, Germany). Three biological replicates
269 of RNA from MM001i and MM008i tumors each were isolated using the Qiagen AllPrep DNA/RNA
270 Mini kit (Qiagen). Tumor tissues were mechanically homogenized in lysis buffer containing β-
271 mercaptoethanol using a glass Dounce homogenizer, followed by repeated aspiration through a
272 syringe for disruption. RNA quality was confirmed by Nanodrop spectrophotometer. Stranded
273 RNA-seq libraries were prepared in collaboration with the Genome Sequencing Facility at UT
274 Health for paired-end 100 bp sequencing. The sequencing raw reads were mapped to the mm10
275 *Mus Musculus* reference genome with HISAT2 v2.1.0[31], and gene counts were calculated with
276 htseq-count. Comprehensive gene expression for cultured cells and tumors of each cell line are
277 available in supplementary table 1. Enrichment of KEGG signaling was conducted using the top

278 1000 expressed genes of each cell line in each condition, with specific focus on immune
279 pathways, cancer cell pathways, and epithelial cell pathways. The input genes and enriched
280 pathways for MM001i and MM008i cultured cells and tumors are available in supplementary table
281 2. Differentially expressed genes in both datasets were identified with DEseq2 v1.40.2[32] by cutoff
282 of log2 fold change > 2 and adjusted *P* value < 0.01 for tumors and < 0.05 in culture.
283

284 **Single-cell expression profiling**

285 Three mammary tumors each of MM001i and MM008i were collected from six individual
286 mice. Single-cell suspensions were prepared for the 10X Genomics Chromium system using a
287 tumor dissociation kit (catalog no. 130-096-730, Miltenyi Biotec, San Diego, CA, USA) at a final
288 concentration of 1000 cells/uL. Single-cell RNA-seq protocol was performed in collaboration with
289 the Genome Sequencing Facility at UT Health according to the technical manual. Raw
290 sequencing reads were aligned to the mouse reference genome mm10 using 10x Genomics Cell
291 Ranger. Feature-barcode matrices were generated with Cell Ranger's count pipeline. Subsequent
292 analysis was performed in Seurat (v4.4.0)[33] using the following workflow: a Seurat object was
293 created with CreateSeuratObject using thresholds of min.cells = 3 (genes detected in ≥3 cells)
294 and min.features = 500 (cells expressing ≥500 genes). Cells with >30% mitochondrial transcript
295 content (percent.mt < 30) were excluded via subset. Clusters were identified using FindClusters
296 with a resolution parameter of 0.5. Cell types were identified manually with curated cell markers:
297 T cells: *Cd3g*, *Cd3d*, *Cd3e*, *Cd247*; B cells: *Cd19*, *B220*; Macrophages: *Cd74*, *Cd14*, *Csf1r*;
298 Endothelial cells: *Esam*, *Pecam1*; Stromal cells: *Fn1*, *Fap*, *Acta2*, *S100a4*; Basal cells: *Krt14*,
299 *Krt5*, *Krt17*; Epithelial cells: *Cdh1*, *Krt8*, *Krt18*, *Krt19*; Cancer cells: *Acta2*, *Aldh1a3*, *Cd24a*, *Cdh1*,
300 *Cdh2*, *Erbb2*, *Kit*, *Krt7*, *Mfge8*, *Myc*, *Pgr*, *Prlr*, *Tjp1*, *Top2a*, *Twist1*.
301

302 **Statistical analysis**

303 Calculations were done using Microsoft Excel software, and statistical analyses were

304 performed using GraphPad Prism software version 10.3.1 (GraphPad, La Jolla, CA, USA). Data
305 were plotted as means ± standard deviation. For tumor growth, Two-way analysis of variance
306 (ANOVA) was used to compare replicate means between multiple groups. Unpaired Student's *t*-
307 test was used to compare individual means. $P < 0.05$ was considered statistically significant.
308

309 **RESULTS**

310 **Generation of murine mammary tumor cell lines MM001i and MM008i**

311 Two spontaneously arising mammary tumors were harvested from independent C57BL/6J
312 *MMTV-Cre p53*$^{fl/+}$ mice, and cell lines were generated by serial passage in culture and *in vivo*
313 (supplementary figure 1A; Materials and Methods). Primary tumors were isolated under sterile
314 conditions and expanded in culture to obtain sufficient cells for cryopreservation and engraftment
315 studies. Five million cells were injected into the mammary fat pad or subcutaneously in severely
316 immunocompromised NSG mice, and tumor formation occurred rapidly within 14-21 days as
317 expected in most animals regardless of injection site (not shown). However, parallel engraftments
318 of 5 x 10^6 cells into the same anatomical locations in fully immunocompetent C57BL/6J (WT)
319 animals only led to tumor formation in the mammary fat pad (supplementary figure 1).
320 Representative tumors from the first mammary fat pad engraftment were expanded in culture and
321 used in a second mammary fat pad engraftment. After two (MM001i) or three (MM008i) rounds of
322 culturing and engraftment, these cell lines formed stable and reproducible mammary tumors
323 (supplementary figure 1D,H). For post-tertiary mammary fat pad engraftments in WT mice, 2.5
324 x10^6 cells were sufficient to form tumors in 21-28 days with at least 70% efficiency. Therefore, this
325 cell number was used for all subsequent experiments.
326

327 **MM001i and MM008i tumors are potential models for human TNBC**

328 As these tumor cell lines had been generated from mice with mammary-specific
329 heterozygosity for *p53*, PCR was used to determine the genotype of this locus (supplementary

330 Figure 2A; primers listed in methods).[28] Although both MM001i and MM008i expressed the *p53*
331 null allele (*i.e.*, *loxP*-to-*loxP* recombined) as anticipated, the WT allele could not be detected.
332 Taken together, these PCR results indicated that both MM001i and MM008i are functionally *p53*
333 homozygous null (likely through loss-of-heterozygosity early in tumor development).

334 Mammary tumor cell lines lacking functional p53 are typically also negative for the hormone
335 receptors, Er, Pr, and Her2.[34, 35] To visualize these cell surface markers, representative tumors
336 from both MM001i and MM008i were formalin-fixed and paraffin-embedded for
337 immunohistochemical staining. MM001i and MM008i are both triple-negative at the protein level,
338 lacking positive nuclear staining of Er[36] and Pr proteins[37] as well as cell surface staining of Her2
339 (supplementary figure 2B).[38]

340 Next, we used flow cytometry to quantify the surface expression of pro-tumorigenic,
341 immune co-signaling molecule Pd-l1 on our cell lines at a basal levels and following 24hrs
342 induction with interferon-gamma (Ifn-γ).[12, 29] MM008i showed higher expression of Pd-l1 at basal
343 levels as well as after Ifn-γ treatment compared to MM001i (supplementary figure 2C). However,
344 cell surface major histocompatibility complex-I (H-2kb) expression was similar between both cell
345 lines regardless of Ifn-γ treatment (supplementary figure 2D).

346

347 **MM001i and MM008i respond differentially to αPD-1 but similarly to αCTLA-4**

348 After establishing a robust mammary fat pad engraftment protocol, WT females were split
349 randomly into subgroups and treated with the two most commonly used immunotherapy agents,
350 αPd-1 and αCtla-4, to gauge therapy responsiveness. After engrafting on day 0 as above,
351 treatment with αPd-1, αCtla-4, or the combination began on day 7, once tumors were
352 approximately 200-300 mm^3. MM001i engrafted animals also received treatments on days 12 and
353 17 (figure 1A). These tumors responded poorly to αPd-1 but regressed completely with αCtla-4
354 monotherapy as well as with αPd-1 + αCtla-4 combination therapy (figure 1B). Non-

355 responsiveness was observed as expected in severely immunocompromised NSG mice (figure
356 1C), indicating that these immunotherapy outcomes are immune response-dependent.
357 MM008i tumors were treated with a single dose on day 7 (Figure 1d). Additional doses
358 were not necessary because tumors regressed rapidly following a single treatment. MM008i
359 tumors responded equally well to both αPd-1 and αCtla-4 monotherapies, ultimately leading to
360 complete tumor regression (figure 1E). The combination of both mAbs appeared to have no
361 additional benefit (figure 1E). The strong responsiveness to αPd-1 monotherapy clearly
362 distinguishes MM008i from MM001i. Moreover, neither tumor line appeared to be immune-cold
363 as evidenced by clear responses to αCtla-4 monotherapy. As for MM001i tumors above, no
364 therapeutic benefit was observed for MM008i in NSG mice in any immunotherapy treatment
365 group, further consistent with an immune response-dependent mechanism of tumor regression
366 (figure 1F).
367
368 **Immunotherapy of MM001i and MM008i tumors generates immune memory**
369 We next asked if immunotherapy treatment of MM001i and MM008i tumors triggers long-
370 lasting immune memory. Mice were engrafted with MM001i and MM008i and, beginning day 7,
371 treated as described above (workflows in figure 2A,C). Mice demonstrating complete tumor
372 regression following αPd-1 and/or αCtla-4 treatment were allowed to rest for 90 days and then
373 rechallenged through injection with the same tumor cell line and same site as in the primary
374 injection. Age-matched female WT mice, which had never been injected with tumor cells
375 previously, were engrafted with MM001i and MM008i as controls. As expected, control mice with
376 *de novo* injections developed mammary tumors in 21-28 days following MM001i or MM008i
377 engraftment (figure 2B,D). Conversely, all previously treated tumor-free mice rejected additional
378 engraftment attempts, thus indicating that both MM001i and MM008i are capable of provoking
379 long-term anti-tumor immune memory.

380

381 **$Cd3^+$ T cells are distributed throughout MM008i unlike MM001i tumors**

382 Although MM001i and MM008i originated from the same genetic background, these two
383 mammary tumor cell lines exhibit starkly different responses to αPd-1 treatment (figure 1). To
384 begin to investigate the underlying mechanism, immunohistochemistry was used to profile tumor-
385 infiltrating immune populations including as B and T lymphocytes. Untreated MM001i and MM008i
386 tumors were isolated after reaching the endpoint tumor volume of 1000 mm^3 and stained for Cd19
387 and Cd3 expression. Based on Cd19 staining, B cell infiltration was low in both MM001i and
388 MM008i tumors (not shown). In contrast, both mammary tumors showed evidence for T cell
389 infiltration with MM008i tumors exhibiting significantly more $Cd3^+$ T lymphocytes compared to
390 MM001i tumors (figure 3A,B; positive control splenic $Cd3^+$ cell staining in supplementary figure
391 3A). Moreover, T cells were localized throughout MM008i tumors versus predominantly around
392 the peripheral margins of MM001i tumors (figure 3A). Deeper T lymphocyte penetration is
393 consistent with the possibility that this cell type may be responsible for the differential αPd-1
394 therapeutic outcomes of MM008i and MM001i tumors.

395

396 **Infiltrating $Cd8^+$ T cells in MM008i tumors**

397 To further profile tumor-associated immune cells, flow cytometry was used to assess
398 specific immune cell subpopulations in treatment-naïve primary tumors. Following live cell gating,
399 a significantly higher percentage of $Cd45^+$ immune cells was identified in MM008i tumors versus
400 MM001i tumors (figure 3C; gating strategy in supplementary figure 3B). There was also a trend
401 toward higher $Cd3^+$ T cells out of $Cd45^+$ immune cells (figure 3D) and, interestingly, a significantly
402 higher percentage of $Cd8^+Cd4^-$ cytotoxic T cells in the $Cd3^+$ population of MM008i tumors (figure
403 3E). Additionally, activated, pre-exhausted $Pd\text{-}1^+Tim3^-Cd8^+$ T cells[12, 39] were significantly higher,
404 though no difference was observed for exhausted $Pd\text{-}1^+Tim3^+$ T cells in MM008i compared to

405 MM001i tumors (figure 3F,G).[40, 41] No significant difference was observed for Cd11b$^+$ monocytes,
406 Cd11b$^+$Gr1$^+$ myeloid-derived suppressor cells, or B220$^+$ B cells (supplementary figure 3C,D,E). A
407 trend towards a higher percentage of Cd11b$^+$Cd11c$^+$ dendritic cells and Nk1.1$^+$ natural killer cells
408 was observed in MM001i tumors, though it was not statistically significant (supplementary figure
409 3F,G). These observations combine to indicate that the successful αPd-1 outcomes observed for
410 MM008i tumor-engrafted animals may be mediated through pre-exhausted Pd-1$^+$Tim3$^-$Cd8$^+$ T
411 cells.
412

413 **Depletion of Cd8$^+$ cells abrogates αPd-1 treatment efficacy in MM008i**

414 The aforedescribed results suggest that the αPd-1 responsiveness of MM008i may be due
415 to infiltrating anti-tumor Cd8$^+$ T cells. To test this possibility directly, experiments were performed
416 in which Cd8$^+$ T cells were immunodepleted from animals before and after MM008i tumor
417 treatment with αPd-1 (workflow in figure 4A). Tumors showed normal growth kinetics in WT
418 animals treated with isotype control mAbs or an αCd8 mAb (figure 4B). As above, αPd-1 treatment
419 alone resulted in near-complete tumor regression (figure 4B). However, three doses of αCd8 mAb
420 (one before and two after αPd-1 treatment) were sufficient to blunt the therapeutic responsiveness
421 of the αPd-1 therapy (Figure 4B). Immunohistochemistry confirmed depletion of Cd8$^+$ T
422 lymphocytes from MM008i tumors (not shown). These data combined to show that Cd8$^+$ T cells
423 are an integral cell population required for MM008i tumor regression in response to αPd-1 therapy
424 in WT mice.
425

426 **RNA-sequencing of MM001i and MM008i cells**

427 To identify tumor-intrinsic factors that contribute to the differential responsiveness to αPd-
428 1, bulk RNA sequencing was done for cultured asynchronous MM001i and MM008i cell
429 populations (2 independent cultures per line) and for untreated tumors from animals (3

430 independent tumors per line). A full list of expressed genes from cultured cells and untreated
431 tumors is provided in supplementary table 1. First, as expected from initial genotyping above, no
432 transcripts were detected for *p53* exons 2-10 confirming *p53* loss of function. Second, multiple
433 breast cancer-associated genes were expressed at similar levels in both cell lines (*Brca1, Brca2,*
434 *Mki67, Myc, Pik3ca*, *Pten*, *Rb1*) with no apparent disease mutations. Third, consistent with IHC
435 results above, *Esr1* transcripts were not detected in either cell line. Fourth, in contrast to the IHC
436 results above where Her2 was not detected, both lines appear to express similar levels of *Erbb2*
437 RNA. This inconsistency may be due to an intrinsic cellular defect prior to translation as this
438 protein was undetectable by IHC and likely not retained intracellularly. Finally, modest levels of *Ar*
439 and *Pgr* RNA were observed in MM001i cultured cells, and not in MM008i. Expression
440 comparisons were less clear in bulk RNA from tumors due to a multitude of normal infiltrating cell
441 types.

442 To evaluate broad expression differences between MM001i and MM008i cells and tumors,
443 we used principal component analysis (PCA) to compare the overall transcription profiles for
444 MM001i and MM008i in each growth condition (supplementary figure 4A). In general, cultured
445 cells clustered closely together as anticipated. In comparison, tumor cells clustered far away from
446 cultured cells and in more loosely associated groups consistent with differential immune
447 responses. We next analyzed specific gene expression differences between MM001i and
448 MM008i, identified based on a greater than 4-fold change and P values < 0.05 for cultured cells
449 and < 0.01 for untreated tumors (figure 5A; supplementary table 1). Among the highest
450 differentially expressed genes are immune related genes, such as *Il11*, *Cxcl2*, *Il7*, *Il1rap*, *Ifnlr1*,
451 and *Cxcl3* in tumors, *Tnf* and *Havcr2* (Tim-3) in cultured cells, and *Il1rl1*, *Nfgr*, and *Ptgs2* in both
452 sets, which could potentially relate to the observed differences in response to αPd-1 therapy and
453 in T lymphocyte infiltration.

454 To evaluate gene expression at the pathway level, we conducted KEGG signaling pathway
455 analysis on the top 1000 expressed genes in MM001i and MM008i cells and tumors, focusing

456 specifically on enriched pathways in immune signaling, cancer, and epithelial cell development
457 (supplementary figure 4B; supplementary table 2). Overall, gene expression was very similar
458 between MM001i and MM008i, particularly in epithelial cell signaling pathways. MM008i tumors
459 were relatively enriched for immune related pathways such as antigen processing and
460 presentation, and phagosome, with genes such as *H2-t23* and *B2m* being among the most
461 strongly expressed. Conversely, MM001i tumors were relatively enriched for cancer related
462 pathways such as extracellular matrix (ECM)-receptor interaction and Pi3k-Akt signaling. These
463 gene expression insights highlight the many similarities between MM001i and MM008i mammary
464 tumor cell models, and also point toward differences that may explain their differential
465 responsiveness to immune therapy.
466

467 **Single-cell profiling of MM001i and MM008i tumors**

468 Single cell (sc)RNA-seq analysis of untreated MM001i and MM008i tumors freshly isolated
469 from mice revealed additional intrinsic and extrinsic features of each tumor cell line. Unsupervised
470 clustering (UMAP) identified major cell types, including normal and cancer epithelial cells,
471 endothelial cells, stromal cells, basal cells, and immune populations (figure 5B,C). Epithelial cells
472 in both MM001i and MM008i exhibited elevated expression of the oncogenes *Myc* and *Top2a*,
473 indicating shared proliferative and malignant transcriptional programs (figure 5D). *Ctla-4* and
474 *Pdcd1* (*Pd-1*) were highly expressed in T cells of both MM001i and MM008i, whereas the mRNA
475 for the Ctla-4 ligand Cd86 showed no significant upregulation in either MM001i or MM008i (figure
476 5D). In contrast, *Cd274* (*Pd-l1*) was overexpressed specifically in epithelial cells of MM008i but
477 not in epithelial cells of MM001i, implying specific immune evasion via the Pd-1/Pd-l1 axis in
478 MM008i tumors (figure 5D).
479

480 **DISCUSSION**

481 We report the development of two syngeneic murine mammary tumor cell lines that,

482 despite originating from the same C57BL/6J genetic background, display differential *in vivo*
483 responsiveness to αPd-1 checkpoint blockade. Specifically, the mammary tumor cell line MM008i
484 tumors responds to αPd-1 therapy and MM001i does not. However, both lines are fully responsive
485 to αCtla-4 therapy, and tumor clearance associates with immunity to subsequent engraftment.
486 Moreover, comparative immune cell profiling of engrafted tumors showed higher percentages of
487 $Cd8^+$ cytotoxic T cells in MM008i tumors compared to MM001i tumors. These $Cd8^+$ T lymphocytes
488 are required for response to αPd-1 in MM008i tumors, as depletion of this population abrogates
489 therapy response. Another key difference we identified was significantly higher expression of Pd-
490 l1 on MM008i epithelial cells compared to MM001i. This strongly indicates that the Pd-1/Pd-l1
491 axis is a major mediator of immune evasion in MM008i, which is reflective of αPD-1 clinical
492 observations in breast cancer where PD-L1 serves as a key biomarker for positive responses.[11,
493 42, 43] However, despite these clear phenotypic differences between tumors, MM001i and MM008i
494 are overall very similar at the gene expression level. We observed similar expression levels of
495 commonly dysregulated breast cancer genes such as *Brca1, Brca2, Mki67, Myc, Pik3ca*, *Pten*,
496 *Rb1*, and *Top2a*, and similarities in epithelial signaling pathways.

497 The mammary tumor models presented help fill an important gap in syngeneic systems
498 for preclinical immune therapy testing and mechanistic studies. Syngeneic mammary tumor
499 models are rare, with only a few described to date.[14, 18, 21, 24-26, 44] E0771, which has been around
500 for 70 years and with unknown passage number, has conflicting reports on Er hormone receptor
501 status.[18] Other lines, such as PyMT,[24] AT-3,[25] and WT145[26] rely on either transgene insertion or
502 chemical carcinogens to drive cancer formation, processes that do not reflect cancer development
503 in human patients. Further, it would be difficult to compare results across lines given substantial
504 differences between each in genetic background, growth kinetics, and immune phenotype, limiting
505 the potential for comparative analysis. To address some of these limitations, recent efforts have
506 focused on developing new models that better recapitulate the immunological characteristics of

507 human disease.[45] However, many of these models are poorly responsive to immunotherapy,
508 owing to low tumor mutational burdens, unless further modified by induced mutagenesis or *Brca1*
509 deficiency.[45] Our models, which exhibit clear responses to αCtla-4 and differential responses to
510 αPd-1, provide a unique platform to dissect mechanisms of immunotherapy resistance and test
511 additional therapies (alone and in combination).

512 In particular, we envision our mammary tumor models being used to test other therapies
513 in combination with αPd-1 for potential dosage de-escalation of MM008i and to potentially trigger
514 αPd-1 responsiveness to MM001i. Our TNBC models also may be used to dissect the tumor
515 microenvironment itself, particularly focusing on extracellular matrix signaling and immune
516 infiltration. Here, we demonstrate considerable differences in T cell infiltration between our
517 MM001i and MM008i tumors. However, we have not directly investigated the specific mechanisms
518 which permit greater immune infiltration in MM008i tumors than MM001i tumors. We anticipate
519 future studies looking more deeply into these two cell lines immunologically, particularly the factors
520 that influence whether a tumor is “immune hot” or “immune cold”. By identifying some of these
521 determinants, we may be able to identify combination therapy approaches to make previously
522 resistant tumors sensitive to immunotherapies.

523

524 **Acknowledgments**

525 We thank Francesca Manara (Memorial Sloan Kettering Cancer Center), Josephine
526 Taverna (UT Health San Antonio), and Ratna Vadlamudi (UT Health San Antonio) for thoughtful
527 feedback, and Emily Law, Jordan Naumann, and Angel Dominguez for early contributions to this
528 project. We are also grateful to Zhao Lai at the UT Health San Antonio Genome Sequencing
529 Facility for assistance with library preparation and sequencing and to the South Texas Research
530 Histology Laboratory for help with mouse specimen processing.

531

Contributors

R.S.H. and H.B.G. conceptualized the project. T.K., H.B.G., C.D., A.S., and B.T. conducted *in vivo* experimentation. X.L., J.P., H.B.G., and I.T. performed immunohistochemistry. T.K., Y.Z., X.L., and N.A.T. contributed computational analyses. T.K. and H.B.G. performed cell-based experiments. T.K., H.B.G. and R.S.H, drafted the manuscript with all authors contributing to manuscript proofing and revision.

Funding

These studies were supported by NCI P50-CA247749, NCI P01-CA234228, and a Recruitment of Established Investigators Award from the Cancer Prevention and Research Institute of Texas (CPRIT RR220053). T.J.K. was supported in part by the STX-MSTP NIH training grants (T32GM113896 and T32GM145432), as well as the Translational Science Training T32 Award (T32TR004545). C.D. was supported in part by a CPRIT Research Training Award (RP 170345). I.T. was also supported in part by NIH T32GM145432. R.S.H. is an Investigator of the Howard Hughes Medical Institute, a CPRIT Scholar, and the Ewing Halsell President's Council Distinguished Chair at the UT Health San Antonio. The UT Health San Antonio Genome Sequencing Facility is supported by NCI P30-CA054174 (Mays Cancer Center at UT Health San Antonio) and NIH Shared Instrument grant S10-OD030311 (S10 grant to NovaSeq 6000 System), and CPRIT Core Facility Award (RP220662). The funders had no roles in study design, data collection and analysis, decision to publish, or preparation of the manuscript.

Competing interests

The authors have no conflicts of interest to declare.

Patient consent for publication

557 Not applicable

558

559 **Provenance and peer review**

560 Not commissioned; externally peer-reviewed

561

562 **Data availability statement**

563 Primary bulk and single-cell RNAseq data sets are available through GEO (GSE305800
564 and GSE305842, respectively). Additional data that support the findings of this study are available
565 from the corresponding author, R.S.H., upon reasonable request.

566

567 **REFERENCES**

568 1. Menon G, Alkabban FM, Ferguson T. Breast cancer. *StatPearls* Treasure Island (FL)2024.

569 2. Nolan E, Lindeman GJ, Visvader JE. Deciphering breast cancer: from biology to the clinic. *Cell*
570 2023;186(8):1708-28.

571 3. Almansour NM. Triple-negative breast cancer: a brief review about epidemiology, risk factors,
572 signaling pathways, treatment and role of artificial intelligence. *Front Mol Biosci*
573 2022;9:836417.

574 4. Dent R, Trudeau M, Pritchard KI, Hanna WM, Kahn HK, Sawka CA, et al. Triple-negative breast
575 cancer: clinical features and patterns of recurrence. *Clin Cancer Res* 2007;13(15 Pt
576 1):4429-34.

577 5. Liedtke C, Mazouni C, Hess KR, Andre F, Tordai A, Mejia JA, et al. Response to neoadjuvant
578 therapy and long-term survival in patients with triple-negative breast cancer. *J Clin Oncol*
579 2008;26(8):1275-81.

580 6. Darb-Esfahani S, Denkert C, Stenzinger A, Salat C, Sinn B, Schem C, et al. Role of TP53
581 mutations in triple negative and HER2-positive breast cancer treated with neoadjuvant
582 anthracycline/taxane-based chemotherapy. *Oncotarget* 2016;7(42):67686-98.

583 7. Cancer Genome Atlas N. Comprehensive molecular portraits of human breast tumours. *Nature*
584 2012;490(7418):61-70.
585 8. Bakhtiar H, Sharifi MN, Helzer KT, Shi Y, Bootsma ML, Shang TA, et al. A phenocopy signature
586 of TP53 loss predicts response to chemotherapy. *NPJ Precis Oncol* 2024;8(1):220.
587 9. Lehmann BD, Bauer JA, Chen X, Sanders ME, Chakravarthy AB, Shyr Y, et al. Identification of
588 human triple-negative breast cancer subtypes and preclinical models for selection of
589 targeted therapies. *J Clin Invest* 2011;121(7):2750-67.
590 10. Schmid P, Cortes J, Pusztai L, McArthur H, Kummel S, Bergh J, et al. Pembrolizumab for early
591 triple-negative breast cancer. *N Engl J Med* 2020;382(9):810-21.
592 11. Cortes J, Rugo HS, Cescon DW, Im SA, Yusof MM, Gallardo C, et al. Pembrolizumab plus
593 chemotherapy in advanced triple-negative breast cancer. *N Engl J Med* 2022;387(3):217-
594 26.
595 12. Nederlof I, Isaeva OI, de Graaf M, Gielen R, Bakker NAM, Rolfes AL, et al. Neoadjuvant
596 nivolumab or nivolumab plus ipilimumab in early-stage triple-negative breast cancer: a
597 phase 2 adaptive trial. *Nat Med* 2024;30(11):3223-35.
598 13. Li Q, Liu J, Zhang Q, Ouyang Q, Zhang Y, Liu Q, et al. The anti-PD-L1/CTLA-4 bispecific
599 antibody KN046 in combination with nab-paclitaxel in first-line treatment of metastatic
600 triple-negative breast cancer: a multicenter phase II trial. *Nat Commun* 2024;15(1):1015.
601 14. Goodson LH, Barvick L, Stone RG, Ibach M, Palmer J. Inhibition screening data using
602 sarcoma 180 and adenocarcinoma E0771. *Cancer Res* 1955;Suppl. 2:81-102.
603 15. Kasikara C, Davra V, Calianese D, Geng K, Spires TE, Quigley M, et al. Pan-TAM Tyrosine
604 Kinase Inhibitor BMS-777607 Enhances anti-PD-1 mAb efficacy in a murine model of
605 triple-negative breast cancer. *Cancer Res* 2019;79(10):2669-83.
606 16. Liu J, Blake SJ, Yong MC, Harjunpaa H, Ngiow SF, Takeda K, et al. Improved efficacy of
607 neoadjuvant compared to adjuvant immunotherapy to eradicate metastatic disease.
608 *Cancer Discov* 2016;6(12):1382-99.

609 17. Zheng X, Fang Z, Liu X, Deng S, Zhou P, Wang X, et al. Increased vessel perfusion predicts
610 the efficacy of immune checkpoint blockade. *J Clin Invest* 2018;128(5):2104-15.
611 18. Le Naour A, Rossary A, Vasson MP. EO771, is it a well-characterized cell line for mouse
612 mammary cancer model? Limit and uncertainty. *Cancer Med* 2020;9(21):8074-85.
613 19. Johnstone CN, Smith YE, Cao Y, Burrows AD, Cross RS, Ling X, et al. Functional and
614 molecular characterisation of EO771.LMB tumours, a new C57BL/6-mouse-derived model
615 of spontaneously metastatic mammary cancer. *Dis Model Mech* 2015;8(3):237-51.
616 20. Gu JW, Young E, Busby B, Covington J, Johnson JW. Oral administration of pyrrolidine
617 dithiocarbamate (PDTC) inhibits VEGF expression, tumor angiogenesis, and growth of
618 breast cancer in female mice. *Cancer Biol Ther* 2009;8(6):514-21.
619 21. Aslakson CJ, Miller FR. Selective events in the metastatic process defined by analysis of the
620 sequential dissemination of subpopulations of a mouse mammary tumor. *Cancer Res*
621 1992;52(6):1399-405.
622 22. Kim K, Skora AD, Li Z, Liu Q, Tam AJ, Blosser RL, et al. Eradication of metastatic mouse
623 cancers resistant to immune checkpoint blockade by suppression of myeloid-derived cells.
624 *Proc Natl Acad Sci U S A* 2014;111(32):11774-9.
625 23. Taylor MA, Hughes AM, Walton J, Coenen-Stass AML, Magiera L, Mooney L, et al.
626 Longitudinal immune characterization of syngeneic tumor models to enable model
627 selection for immune oncology drug discovery. *J Immunother Cancer* 2019;7(1):328.
628 24. Yan C, Yang J, Saleh N, Chen SC, Ayers GD, Abramson VG, et al. Inhibition of the PI3K/mTOR
629 pathway in breast cancer to enhance response to immune checkpoint inhibitors in breast
630 cancer. *Int J Mol Sci* 2021;22(10).
631 25. Stewart TJ, Abrams SI. Altered immune function during long-term host-tumor interactions can
632 be modulated to retard autochthonous neoplastic growth. *J Immunol* 2007;179(5):2851-9.
633 26. Zinser GM, McEleney K, Welsh J. Characterization of mammary tumor cell lines from wild
634 type and vitamin D3 receptor knockout mice. *Mol Cell Endocrinol* 2003;200(1-2):67-80.

635 27. Percie du Sert N, Hurst V, Ahluwalia A, Alam S, Avey MT, Baker M, et al. The ARRIVE
636 guidelines 2.0: updated guidelines for reporting animal research. *BMJ Open Sci*
637 2020;4(1):e100115.
638 28. Marino S, Vooijs M, van Der Gulden H, Jonkers J, Berns A. Induction of medulloblastomas in
639 p53-null mutant mice by somatic inactivation of Rb in the external granular layer cells of
640 the cerebellum. *Genes Dev* 2000;14(8):994-1004.
641 29. Gupta HB, Clark CA, Yuan B, Sareddy G, Pandeswara S, Padron AS, et al. Tumor cell-intrinsic
642 PD-L1 promotes tumor-initiating cell generation and functions in melanoma and ovarian
643 cancer. *Signal Transduct Target Ther* 2016;1:16030-.
644 30. Durfee C, Temiz NA, Levin-Klein R, Argyris PP, Alsoe L, Carracedo S, et al. Human
645 APOBEC3B promotes tumor development in vivo including signature mutations and
646 metastases. *Cell Rep Med* 2023;4(10):101211.
647 31. Kim D, Paggi JM, Park C, Bennett C, Salzberg SL. Graph-based genome alignment and
648 genotyping with HISAT2 and HISAT-genotype. *Nat Biotechnol* 2019;37(8):907-15.
649 32. Love MI, Huber W, Anders S. Moderated estimation of fold change and dispersion for RNA-
650 seq data with DESeq2. *Genome Biol* 2014;15(12):550.
651 33. Hao Y, Hao S, Andersen-Nissen E, Mauck WM, 3rd, Zheng S, Butler A, et al. Integrated
652 analysis of multimodal single-cell data. *Cell* 2021;184(13):3573-87 e29.
653 34. Knight JF, Lesurf R, Zhao H, Pinnaduwage D, Davis RR, Saleh SM, et al. Met synergizes with
654 p53 loss to induce mammary tumors that possess features of claudin-low breast cancer.
655 *Proc Natl Acad Sci U S A* 2013;110(14):E1301-10.
656 35. Wang S, Liu JC, Kim D, Datti A, Zacksenhaus E. Targeted Pten deletion plus p53-R270H
657 mutation in mouse mammary epithelium induces aggressive claudin-low and basal-like
658 breast cancer. *Breast Cancer Res* 2016;18(1):9.

659 36. Bruner-Tran KL, Duleba AJ, Taylor HS, Osteen KG. Developmental toxicant exposure is
660 associated with transgenerational adenomyosis in a murine model. *Biol Reprod*
661 2016;95(4):73.
662 37. Zhao W, Wang Y, Liu J, Yang Q, Zhang S, Hu X, et al. Progesterone activates the histone
663 lactylation-Hif1alpha-glycolysis feedback loop to promote decidualization. *Endocrinology*
664 2023;165(1).
665 38. Choudhury S, Ghosh S, Chakraborty P, Pal S, Ghosh K, Saha S, et al. Epidermal growth
666 factor receptor (EGFR) and SMAD4 negatively correlated in the progression of gallbladder
667 cancer in Eastern Indian patients. BMC Gastroenterol 2024;24(1):446.
668 39. Kinget L, Naulaerts S, Govaerts J, Vanmeerbeek I, Sprooten J, Laureano RS, et al. A spatial
669 architecture-embedding HLA signature to predict clinical response to immunotherapy in
670 renal cell carcinoma. *Nat Med* 2024;30(6):1667-79.
671 40. Jin HT, Anderson AC, Tan WG, West EE, Ha SJ, Araki K, et al. Cooperation of Tim-3 and PD-
672 1 in CD8 T-cell exhaustion during chronic viral infection. *Proc Natl Acad Sci U S A*
673 2010;107(33):14733-8.
674 41. Sakuishi K, Apetoh L, Sullivan JM, Blazar BR, Kuchroo VK, Anderson AC. Targeting Tim-3
675 and PD-1 pathways to reverse T cell exhaustion and restore anti-tumor immunity. *J Exp*
676 *Med* 2010;207(10):2187-94.
677 42. James JL, Balko JM. Biomarker predictors for immunotherapy benefit in breast: beyond PD-
678 L1. *Curr Breast Cancer Rep* 2019;11(4):217-27.
679 43. Khan M, Du K, Ai M, Wang B, Lin J, Ren A, et al. PD-L1 expression as biomarker of efficacy
680 of PD-1/PD-L1 checkpoint inhibitors in metastatic triple negative breast cancer: A
681 systematic review and meta-analysis. *Front Immunol* 2023;14:1060308.
682 44. Perez-Lanzon M, Carbonnier V, Cordier P, De Palma FDE, Petrazzuolo A, Klein C, et al. New
683 hormone receptor-positive breast cancer mouse cell line mimicking the immune

684 microenvironment of anti-PD-1 resistant mammary carcinoma. *J Immunother Cancer*
685 2023;11(6).
686 45. Hollern DP, Xu N, Thennavan A, Glodowski C, Garcia-Recio S, Mott KR, et al. B cells and T
687 follicular helper cells mediate response to checkpoint inhibitors in high mutation burden
688 mouse models of breast cancer. *Cell* 2019;179(5):1191-206 e21.
689
690

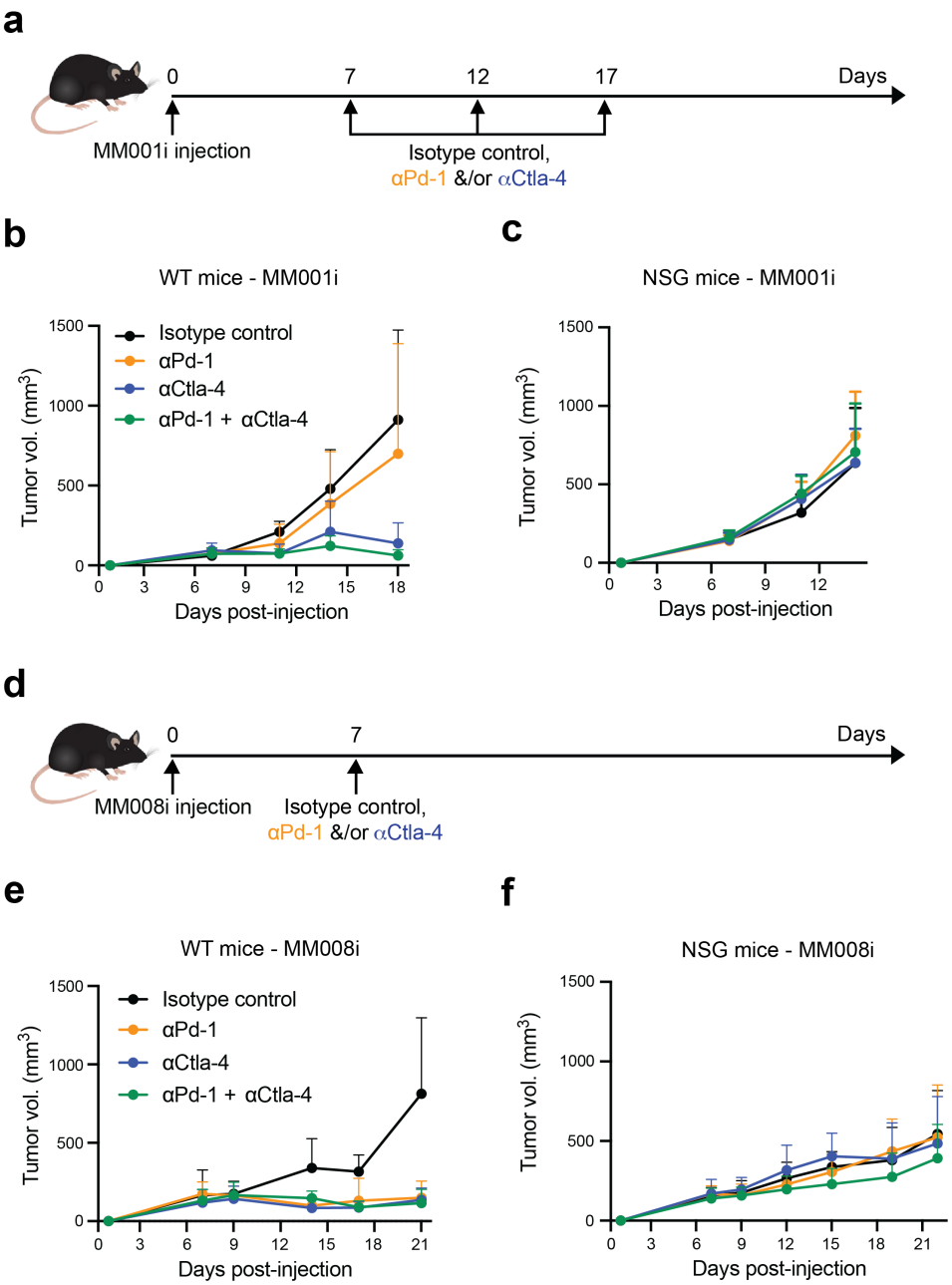

Figure 1. MM001i and MM008i tumors exhibit differential immunotherapy responsiveness.

(**a**) Timeline of MM001i tumor injection and treatment with αPd-1 ± αCtla-4 or isotype controls. (**b-c**) Tumor growth curves of MM001i following injection into the mammary fat pads of WT or severely immunocompromised (NSG) female mice, respectively, in the indicated treatment groups. n=6 (WT) or 4 (NSG) animals per group with two tumors per mouse; *P*-values using two-way ANOVA.

(**d**) Timeline of MM008i tumor injection and treatment with αPd-1 ± αCtla-4 or isotype controls. (**e-f**) Tumor growth curves of MM001i following injection into the mammary fat pads of WT or NSG female mice, respectively, in the indicated treatment groups. n=6 (WT) or 4 (NSG) animals per group with two tumors per mouse; *P*-values using two-way ANOVA.

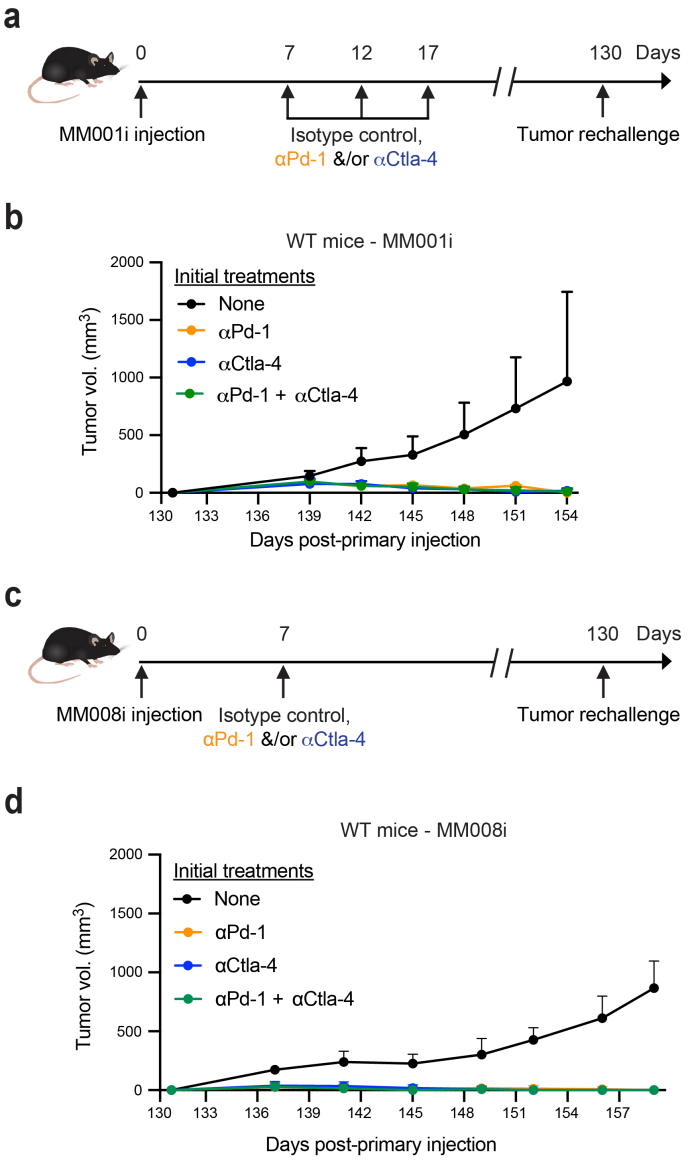

Figure 2. MM001i and MM008i tumors elicit durable immune memory response post-immunotherapy treatments.

(**a**) Timeline of initial and subsequent MM001i tumor injections and treatment with αPd-1, αCtla-4, or combination.

(**b**) Tumor growth curves of MM001i following second tumor engraftment into WT female mice. n=4 animals per group (1 mouse for αPd-1) with two tumors per mouse; *P*-values using two-way ANOVA.

(**c**) Timeline of initial and subsequent MM008i tumor injections and treatment with αPd-1, αCtla-4, or combination.

(**d**) Tumor growth curves of MM008i following second tumor engraftment into WT female mice. n=5 animals per group with two tumors per mouse; *P*-values using two-way ANOVA.

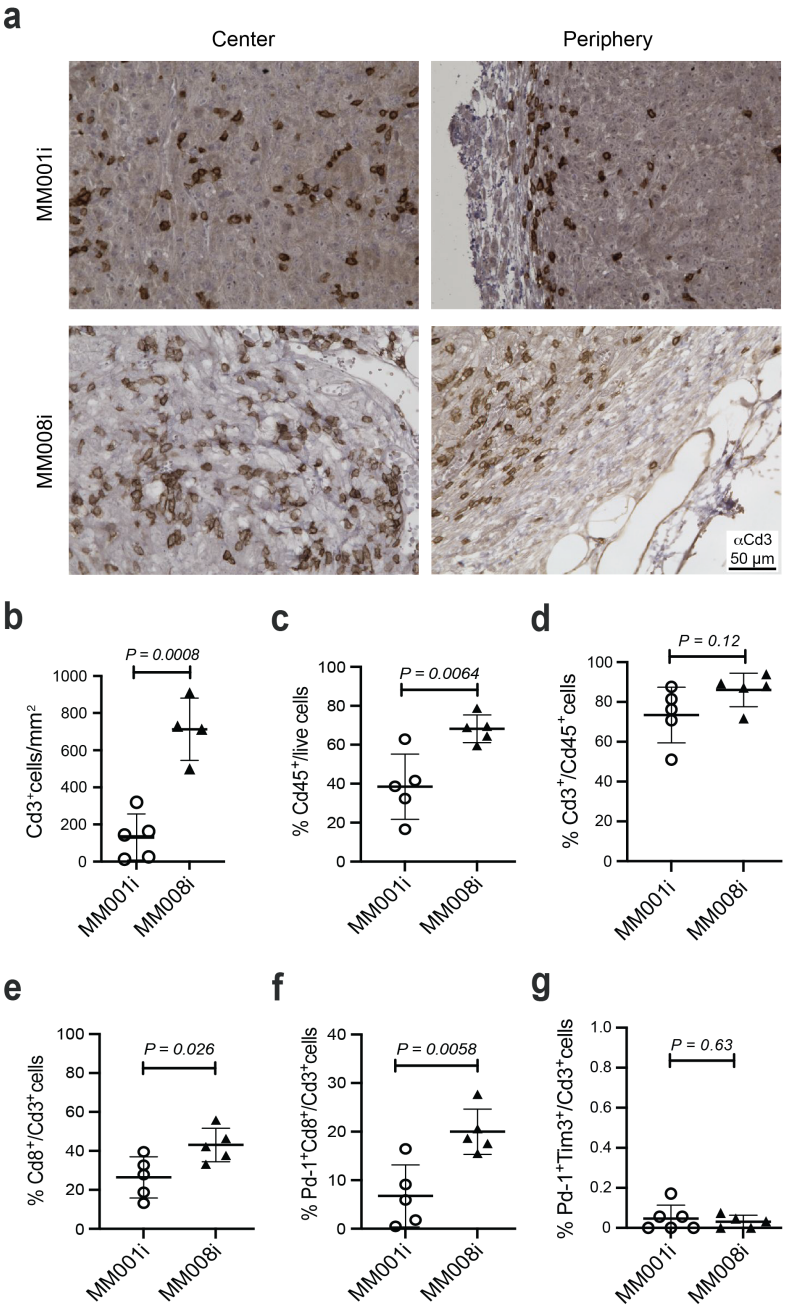

Figure 3. MM008i tumors are enriched with total T cells and pre-exhausted Pd-1$^+$Cd8$^+$ T cells compared to MM001i tumors.

(**a**) Representative αCd3 IHC images of untreated MM001i and MM008i tumors.

(**b**) Quantification of Cd3$^+$ T cells/mm^3 in untreated MM001i and MM008i tumors using QuPath bioimage analysis software (5 random uniform regions of interest per tumor; n=5 tumors for MM001i, and 4 tumors for MM008i; *P* value by unpaired Student's *t*-test).

(**c-g**) Immune cell infiltrates with the indicated cell surface markers as estimated by flow cytometry (n=4-5 tumors per group; *P* value by unpaired Student's *t*-test).

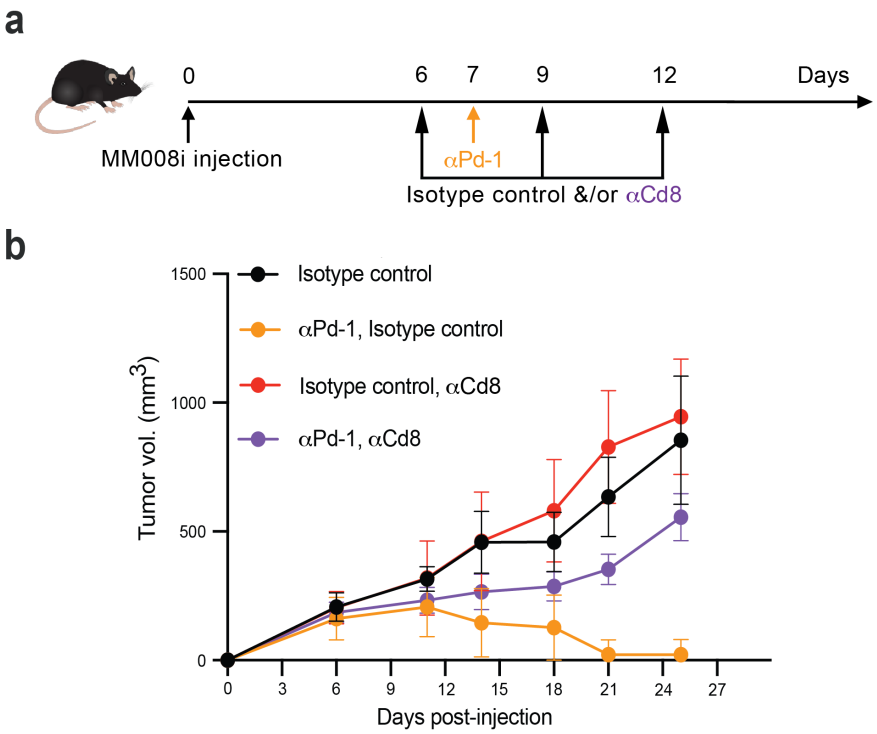

723

724 **Figure 4.** αCd8 neutralizing antibody abrogates αPd-1 response in MM008i tumors.

725 (**a**) Timeline of MM008i tumor injections and treatments with αPd-1 ± αCd8 or isotype controls.

726 (**b**) Tumor growth curves of MM008i following tumor injection in WT females in the indicated
727 treatment groups. n=5 animals per group with two tumors/mouse; *P*-values using two-way
728 ANOVA.

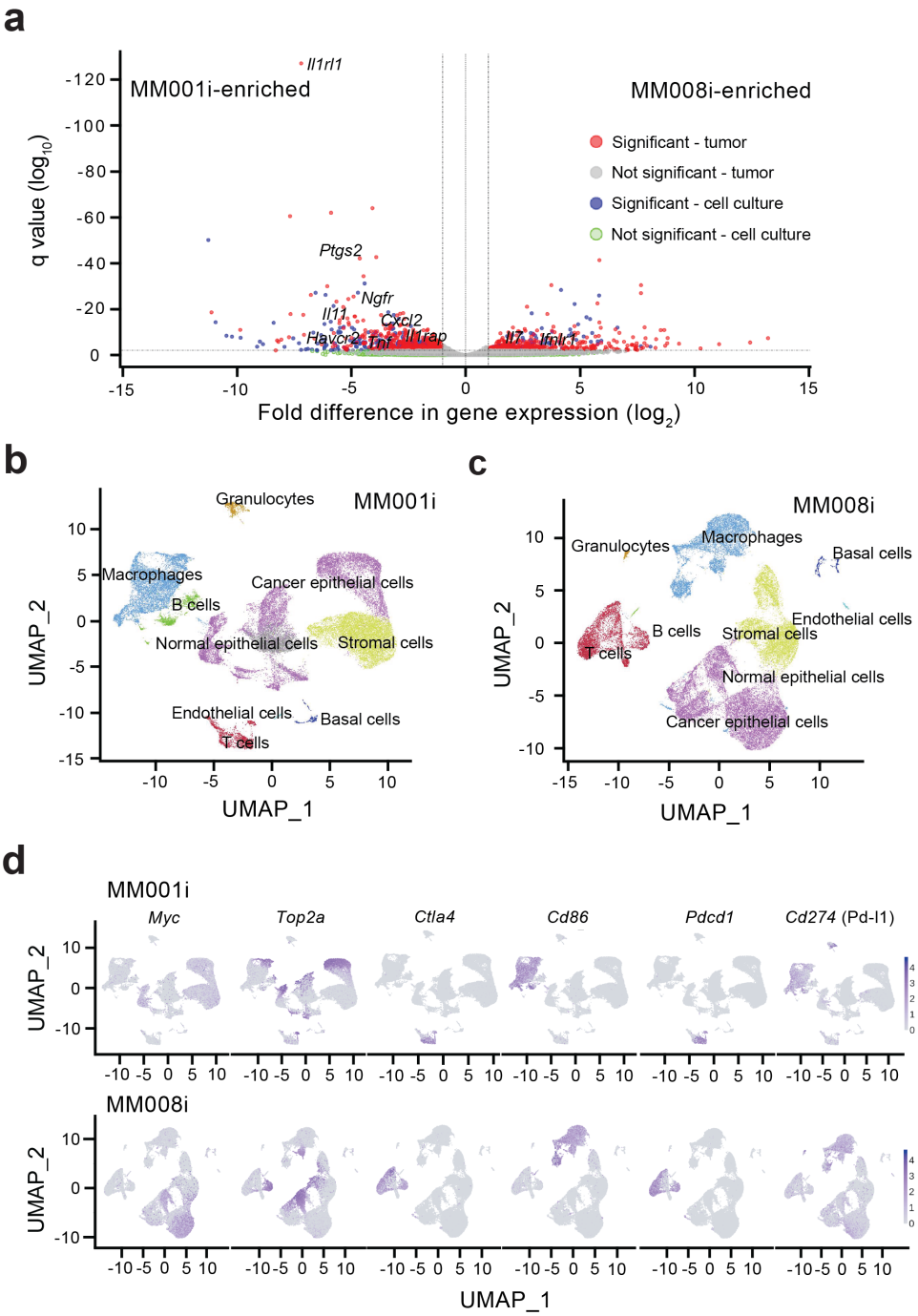

Figure 5. Gene expression profiling of MM001i and MM008i tumors.

(**a**) Volcano plot depicting differentially expressed genes between MM001i and MM008i cells in culture and tumors *in vivo* by RNA-seq (filtered by $\log_2$-fold change > 2 and adjusted *P*-value <0.05 for cultured cells and < 0.01 for tumors)**.**

(**b-c**) UMAP clustering of MM001i and MM008i tumors, respectively, with cell type annotations by single-cell RNA-seq.

(**d**) Expression distributions for *Myc*, *Top2a*, *Ctla4*, *Cd86*, *Pdcd1*, and *Cd274* at the single cell level in MM001i and MM008i tumors overlaid upon respective UMAPs.